



Turbine Aerodynamic Low-Frequency Oscillation and Noise Reduction Using Partial Shrouds

Patrick S. Rebholz,* Simon Krebietke,† and Reza S. Abhari‡
Swiss Federal Institute of Technology, 8092 Zurich, Switzerland
and
Anestis I. Kalfas§
Aristotle University of Thessaloniki, 54124 Thessaloniki, Greece

DOI: 10.2514/1.B36031

The design of highly efficient low-pressure gas turbines in compliance with strict emission regulations for pollutants and noise, as well as long component lifetime, requires the detailed knowledge of potential excitations in the flow. The analysis of fast response measurement data from a 1.5-stage low-pressure axial turbine in the frequency domain shows multiple relevant excitation and noise sources in the flowfield, in addition to the primary rotor–stator interaction. Especially nonsynchronous low-frequency modes at 10% of the blade-passing frequency, occurring in the tip shroud exit cavity, are found to communicate with the main flow and are amplified through the downstream stator row by a flow instability in the interaction area of the passage vortex and boundary layer. Full-annular unsteady computational fluid dynamics simulations are carried out in addition to the experiments to probe the origin of the cavity modes. They predict the rotor–stator interaction well, but they struggle to resolve low-frequency oscillations in the cavities. Out of the four tested configurations, a shroud trailing-edge cutback is the most efficient option to prevent the formation of the cavity modes. The tradeoff for a low-frequency fluctuation reduction of 12 dB using a trailing-edge partial shroud is a total–total stage efficiency drop of 0.7%.

Nomenclature

C_{ax}	=	axial chord
f	=	frequency
\dot{m}	=	mass flow
N	=	rotational speed
p	=	pressure
Re	=	Reynolds number
T	=	temperature
v	=	velocity
η	=	efficiency
λ	=	wavelength
Π	=	pressure ratio

Subscripts

in	=	turbine inlet
max	=	maximum
RMS	=	root mean square
0	=	stagnation flow quantity
1.5	=	across 1.5 stages

I. Introduction

JET engines are among the most sophisticated and multidisciplinary devices built today. The temperature and stress levels in different parts of the engine have been pushed in order to achieve more efficient aircraft propulsion. Typically, the interaction of different optimization goals in aerodynamics, thermodynamics, and structural mechanics results in a tradeoff. The superior aerodynamic efficiency and the

mitigation of blade flutter are two main reasons for the wide use of shrouded blades in low-pressure turbines [1]. However, for the new generation of high-speed low-pressure turbines, the shroud weight has a significant impact on fatigue life. The quadratic increase in mean stress for higher rotational speeds results in lower allowable stress amplitudes, and therefore the first representatives of this engine family feature unshrouded low-pressure turbine blades (2,3). Especially for high-pressure turbines, a big variety of literature has been published on tip treatment, since the cooling fluid required to keep the shroud within acceptable temperatures has a major impact on the overall efficiency. Harvey [4] presented the most comprehensive overview on blade tip design. It was shown qualitatively that the resulting loss as a function of tip gap was twice as high for unshrouded turbines when compared to shrouded designs. Squealer geometries have been studied as alternatives to shrouds by Kaiser and Bindon [5], Camci et al. [6], Mischo et al. [7], and others. Similar to the winglet geometries studied by Dey and Camci [8] and Zhou et al. [9], the tip squealers do not provide additional stiffness to a blade row.

Partial shrouds therefore represent a potential solution providing a compromise between aerodynamic benefits and structural drawbacks. Aerodynamic effects of partial shrouds have been studied by Nirmalan and Bailey [10] in a cascade with three different scallop designs. As in the work done by Porreca et al. [11], they found aerodynamic efficiency reductions on the order of 1% compared to a full shroud. The aerodynamic behaviors of the four shroud geometries under consideration in this paper were studied in a previous publication by Rebholz et al. [12]. The main findings relevant for this paper were the interaction of the overtip leakage with the main flow and the propagation through the downstream stator row. For both leading-edge (LE) and trailing-edge (TE) cutbacks, the total amount of leakage was estimated numerically to remain constant, but the fluid exchange in the according cavities was enhanced by factors of up to two. Since the pumping was determined by the rotor pressure field, the flowfield in the cavity was also influenced more by the rotor motion than the dynamics of the toroidal vortex systems, as in the fully shrouded case. Tracking fluid with enhanced total temperature allowed identification of the dominant outflow locations from the shroud exit cavity in the middle of the second stator (denoted as S2) passage. The leakage fluid appeared to accumulate on the suction side (SS) of the second stator down to 40% of the blade span.

All of the previously cited studies focused mainly on performance. However, potential high cycle fatigue sources as well as strict noise

Received 1 October 2015; accepted for publication 27 May 2016; published online 9 August 2016. Copyright © 2016 by the American Institute of Aeronautics and Astronautics, Inc. All rights reserved. Copies of this paper may be made for personal and internal use, on condition that the copier pay the per-copy fee to the Copyright Clearance Center (CCC). All requests for copying and permission to reprint should be submitted to CCC at www.copyright.com; employ the ISSN 0748-4658 (print) or 1533-3876 (online) to initiate your request.

*Research Assistant, Laboratory for Energy Conversion; rebholz@lec.mavt.ethz.ch (Corresponding Author).

†Research Assistant, Laboratory for Energy Conversion.

‡Professor, Laboratory for Energy Conversion.

§Professor, Department of Mechanical Engineering.

emission regulations require an analysis beyond integral quantities like efficiency. Fortunately, the noise signature of turbofans improves along with the increasing bypass ratio, since the emitted jet noise scales to the eighth power of the exhaust velocity, as shown by Bushell [13] already in 1971. However, tonal noise like the blade-passing frequency of the rows is still critical, especially during landing and takeoff, when the engines are pointed toward the ground. The highly unsteady nature of various other flow features creating tonal noise is difficult to capture experimentally and computationally. The cavities required for the integration of shrouded blades need to be designed primarily for clearance. In addition to the forcing created by the interaction of the leakage and main flow, shown by Gezork et al. [14], such enclosed volumes are susceptible to acoustic resonance and exhibit highly unsteady vortex dynamics, which have been analyzed by Barmपालias et al. [15] and others. The presence of highly swirling flows and vortical structures can also introduce instabilities, which have been studied analytically and numerically (Blackburn and Lopez [16] and Globulev and Atassi [17]). The complexity of this problem, which is derived from the curl of the Navier–Stokes equations, typically leads to a mathematical treatment and a simplification of the engine environment.

Due to the relation to the blade position, the rotor–stator interaction is typically well captured by numerical methods that are integrated in the design process. The underlying dynamics for the previously mentioned instabilities can result in nonsynchronous fluctuations, which are not captured by standard numerical methods, especially periodic sector reductions of the full geometry. Periodic boundary conditions act as high-pass filters in circumferential direction, and therefore may prevent the buildup of nonsynchronous dynamics potentially found in cavities, as shown by Basol et al. [18]. Especially noise generation depends on the nonlinear nature of the Navier–Stokes equations, and typical acoustic sources like the Reynolds stresses have to be modeled accordingly. Karbasov et al. [19] treated them as source terms to determine the evolution of jet noise through an exhaust nozzle. More recently, hybrid Reynolds-averaged Navier–Stokes (RANS)/large-eddy simulation codes are used, like by Nebenfuehr et al. [20].

Given the aforementioned challenges in fatigue- and noise-related problems, this paper presents an extended analysis of experimental results and a numerical approach to capture flow oscillations related to structural excitation and noise generation in cavities. The experimental data of four different shroud geometries have been transformed into the frequency domain at multiple measurement points in order to capture the whole frequency content of the signal rather than engine-order components only. Using this approach in combination with tip shroud cavity instrumentation, a nonsynchronous low-frequency oscillation generated in the shroud exit cavity can be detected and traced through the turbine. The low damping characteristics through a stage, as well as potential excitation of other flow instabilities, may lead to significant low-frequency vibrations and noise emissions. The nonacoustic nature of this cavity mode gives rise to a full-annular unsteady RANS simulation that does not suppress the buildup of such a mode in pitchwise direction. The impact of first-engine-order fluctuations in the proximity of the shroud seals caused by manufacturing and assembly tolerances, which is dominant in the seal gap region, is not modeled in this simulation and leads to a deviation in the cavity frequency.

Partial shrouds emerge from the analysis as a viable option to reduce weight, and therefore potentially mean blade stress compared to a full shroud, while still benefitting from the superior aerodynamics and the robustness against flutter compared to unshrouded blades. The openings in the shroud platform lead to a dominance of the rotor pressure field rather than more independent cavity dynamics as for a full shroud. A shroud trailing-edge cutback also suppresses the generation of low-frequency pressure oscillations in the cavities by up to 12 dB at the exit of the turbine compared to a full shroud.

II. Experimental Method

The experimental investigation was performed in the “LISA” research turbine at the Laboratory for Energy Conversion (LEC) at

the Swiss Federal Institute of Technology in Zurich. A detailed description was presented by Behr et al. [21].

A. Research Turbine Facility

The research turbine shown in Fig. 1 is a quasi-closed-loop facility. The inlet pressure is generated by a radial compressor. The inlet total temperature $T_{0,in}$ is controlled to ± 0.2 K with a two-stage water-to-air heat exchanger, and the mass flow is measured with a calibrated Venturi nozzle. A homogeneous flowfield is created by a 3 m flow conditioning stretch before the flow enters the test section. The acceleration in the contraction helps reduce flow nonuniformities. The flow undergoes a subatmospheric expansion through 1.5 stages. After the pressure is recovered to the atmospheric level, the air loop is open to atmosphere downstream of the turbine. The recovery of the static pressure with a tandem deswirl vane row is required due to the compressor’s limited compression of $\Pi_{c,max} = 1.4$. The rotational speed of the turbine of 2700 rpm is controlled by a dc generator to an accuracy of ± 0.5 rpm. The turbine torque is measured by a torque meter. The first vane row exit flow is compressible with a Mach number of 0.52.

B. Operating Conditions

The total-to-static pressure ratio across the 1.5-stage test section is kept constant for all measurements at $\Pi_{1,5} = 1.65$. The inlet total temperature is also kept constant at $T_{0,in} = 328$ K. A constant amount of purge flow of 0.8% of the main mass flow (typically 11.8 kg/s) is injected at the hub between the first vane and the rotor. The injection system was described in more detail by Schuepbach et al. [22]. Due to the opening to the atmosphere at the exit of the turbine, all thermodynamic flow quantities are normalized by the inlet stagnation conditions. This procedure allows for an accurate comparison between different measurement days. The operating characteristics are summarized in Table 1.

C. Shroud Cutback Designs

The turbine configuration is based on the design used by Jenny et al. [23]. The endwalls of the first vane row are profiled at the hub and tip, whereas the second vane has cylindrical endwalls. The hub endwall profiling as well as the blade geometry of the rotor are identical to previous experiments and are the same for all cutback

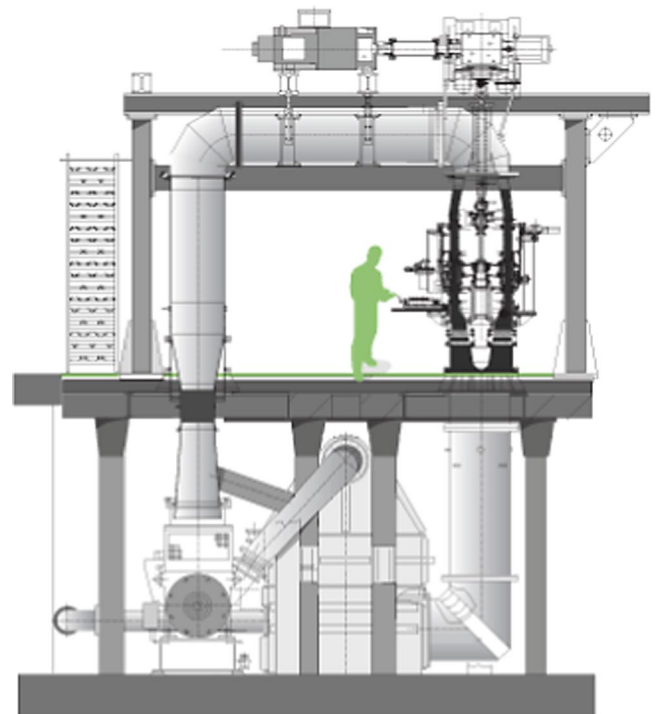


Fig. 1 Overview of the LISA test facility at the Laboratory for Energy Conversion at ETH in Zurich.

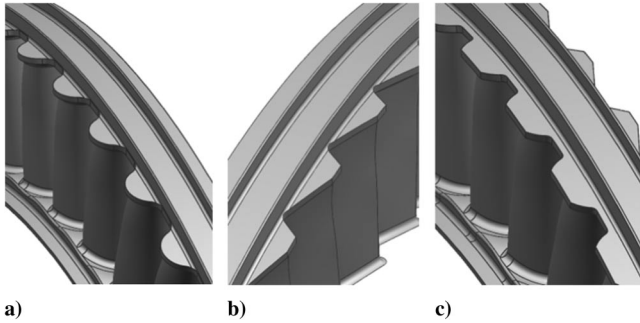


Fig. 2 Three tested shroud cutback geometries: a) leading-edge cutback, b) trailing-edge cutback, and c) combined cutback.

designs. For the baseline, the shroud features a cylindrical endwall to allow for modifications. To provide more space for the shroud leading-edge modification, the first sealing fin is placed at 5% of the axial cavity length (7% of the rotor tip axial chord) away from the cavity inlet, increasing the inlet cavity volume by 17%. The shroud leading-edge platform is then reduced to the fillet of the blade, leaving a semicircular platform. This is an engine representative design and is referred to as the LE cutback in this paper. For this case, 11.6% of the total shroud material is removed. The geometry is shown in Fig. 2a. A separate rotor featuring a partial shroud at the trailing edge, referred to as the TE cutback, is designed based on the findings of Porreca et al. [24]. As shown in Fig. 2b, the shroud trailing-edge platform is cut back to the maximum extent while leaving the throat area of the turbine and the fillet unaltered. The overall material reduction equals 5.3% for this design, i.e., less than half compared to the LE cutback. The goal for the combined cutback was to have the same weight, and therefore potentially the same stress reduction as for the LE cutback. The shroud trailing-edge modification is identical to the TE cutback, but the shroud leading-edge modification has an axial offset compared to the LE cutback.

D. Measurement Planes

The traverse data presented in this paper were acquired downstream of the rotor and downstream of the second stator, as shown in Fig. 3. The spatial resolution of the measurement grid covered 42 radial and 41 equally spaced circumferential points covering one stator pitch. The radial resolution was refined close to the endwalls.

Pneumatic tappings and pressure transducers were installed on the outer tip shroud cavity wall. In the inlet cavity (denoted as 1) and the exit cavity (denoted as 3) in Fig. 4, the axial resolution of the tappings is 3% of the axial cavity dimension and 6% for the transducers, respectively.

E. Measurement Technology

The performance of the different cutback configurations is derived from the steady flowfield, which is measured with a cobra-shaped pneumatic five-hole probe (5HP) with a head diameter of 0.9 mm. The unsteady flowfield is captured with a two-sensor fast response aerodynamic probe (FRAP), which was developed at the Swiss

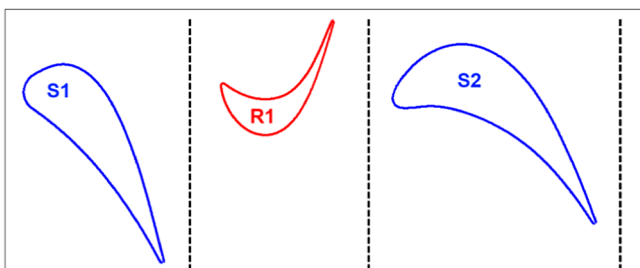


Fig. 3 Sketch of the measurement plane locations upstream and downstream of the rotor and downstream of the second stator (R1 denotes first turbine rotor).

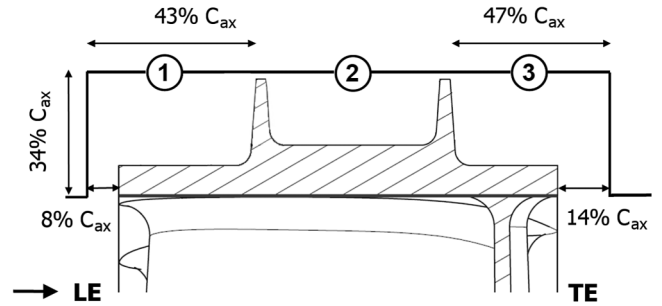


Fig. 4 Sketch of the rotor tip shroud cavity.

Federal Institute of Technology (ETH) in Zurich (Kupferschmied et al. [25] and Pfau et al. [26]), and has a head diameter of 1.8 mm. The FRAP probe resolves flowfield oscillations with frequencies up to 48 kHz. It is operated in a virtual four-sensor mode, allowing the measurement of the three-dimensional and time-resolved flowfield. Table 2 shows the relative uncertainty of the 5HP and FRAP relative to the calibration range of ± 30 deg for the yaw angle, ± 20 deg for the pitch angle, and as a percentage of the dynamic head for the total and static pressure. Three consecutive rotor blade passings are considered in the standard postprocessing and phase-lock averaged 85 times. The data are acquired at a sampling rate of 200 kHz over a period of 2 s, which results in a frequency resolution in the frequency domain of 0.5 Hz. For the frequency domain analysis, only the pressure signal from the yaw sensor in the probe position aligned to the mean flow direction is considered. The signal therefore resembles the total pressure and contains the full frequency spectrum rather than engine orders only, as in the phase-lock averaged case. Flow incidences other than 0 deg relative to the pressure holes caused by transient yaw angle variations are also recorded as pressure fluctuations on the yaw sensors. Based on the phase-lock-averaged results, deviations from the total pressure due to flow angle variations are estimated to be, at most, 1.5% of the inlet total pressure, but typically less than 0.2% for all measurement planes.

The uncertainty of the pneumatic tapping measurements of the static wall pressure on the outer shroud cavity wall is estimated to be 0.02% of the inlet total pressure. The expanded uncertainty for the time-resolved wall pressure measurements was estimated to be 0.1% of the inlet total pressure by Behr [27]. The unsteady wall pressure is recorded with a sampling rate of 100 kHz for 3 s, resulting in a frequency resolution of 1/3 Hz.

III. Computational Method

A. Grid and Boundary Conditions

To not restrict the flow behavior by periodic boundary conditions, the computational domain of the baseline covers the full annulus of a 1.5-stage configuration. The mesh of the time-resolved simulations is created in the commercial mesh generator "ANSYS IcemCFD" and consists of approximately 100 million nodes. It is refined in the areas of interaction in the tip shroud cavity and uses matching interfaces in order to minimize interpolation errors at both the stage interfaces as well as at the shroud. The simulations do contain the hub rim seal upstream of the rotor, but zero net purge flow is injected. The impact of the purge flow on the tip shroud cavity is marginal, since it only affects the flowfield up to a 60% span [23].

The boundary conditions at the inlet and the outlet of the turbine are extracted from performance measurements. At the domain inlet, the total pressure and total temperature are specified accordingly. The turbulence intensity is set to 0.5% in the main flow upstream of the first stator (denoted as S1). The exit static pressure is fixed at the hub and follows a radial equilibrium distribution along the span.

B. Solver

The current numerical study is conducted using LEC's in-house graphics processing unit (GPU) accelerated compressible unsteady RANS solver "MULTI3." The numerical algorithm is based on Ni's Lax-Wendroff [28] explicit time-marching scheme, which has

Table 1 Rig operating conditions

Parameter	Value
$\Pi_{1.5}$	$1.65 \pm 0.4\%$
$T_{0,in}$, K	328 ± 0.3
$\dot{m} \sqrt{T_{0,in}} / p_{0,in}$, $\text{kg} \cdot \text{K}^{0.5} \cdot \text{s}^{-1} \cdot \text{bar}^{-1}$	152 ± 0.2
$N / \sqrt{T_{0,in}}$, round per second $\cdot \text{K}^{-0.5}$	2.48 ± 0.05
Mach number (S1 exit/Rotor 1 exit/S2 exit)	0.52/0.28/0.48
Reynolds number (S1/R/S2)	$7.1/3.8/5.1 \times 10^5$

Table 2 Relative uncertainty of the SHP and the FRAP

	Yaw, %	Pitch, %	p_0 , %	p , %
5HP	0.5	0.8	0.6	1.0
FRAP	0.8	2.3	1.0	1.2

second-order accuracy in both space and time. Turbulence closure is obtained using the Wilcox $k-\omega$ turbulence model. The solver was described in detail by Basol et al. [18].

A full revolution is discretized by 540 physical time steps using 150 subiterations. The initial condition for the full-annular simulation is taken from a converged sector model of the domain. The computation is carried out on 18 GPUs.

C. Validation

The convergence of the simulation has been judged based on the periodic correlation between two blade passings at midspan in the main flow at the exit of each stage. However, the presence of non-periodic flow features in the cavities prevented a conclusive statement on complete convergence.

Figure 5 shows a comparison between the experiment and the computation of the mass-averaged relative total pressure and relative yaw angle at the rotor exit for the baseline. Since the flowfield was found to be affected by the purge flow injection up to a 60% span, only the tip part of the curves was considered for the validation. Here, the relative total pressure showed good agreement and deviations of less than 0.5%. The underturning caused by the rotor tip passage vortex at 85% span was underpredicted by computational fluid dynamics (CFD). The deviation of the flow yaw angle was less than 2 deg above the 60% span. In the hub region below the 30% span, the impact of the higher purge flow from the experiment could be noticed clearly. The pressure drop across the first shroud fin was captured well by CFD. However, the rotor inlet static pressure was underpredicted by approximately 0.8%, as shown in Fig. 6. This offset was

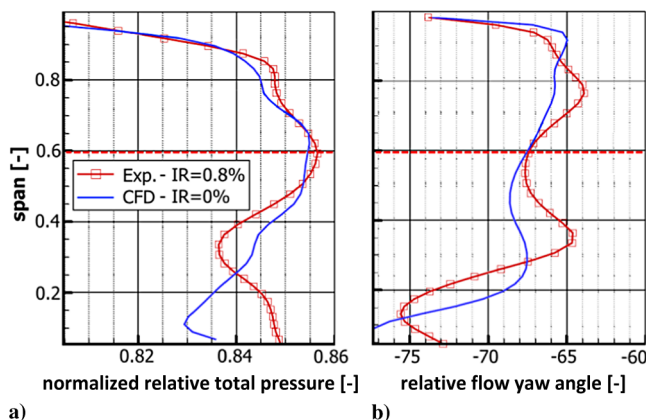


Fig. 5 Comparison between CFD and experiment (Exp.) at rotor exit for the baseline, circumferentially mass-averaged a) normalized relative total pressure and b) relative flow yaw angle.

also seen in the intermediate cavity, so the pressure drop across the second fin was underestimated by approximately 1%.

IV. Results and Discussion

The general flowfield and the aerodynamic impact of different tip shroud cutbacks was discussed by Rebholz et al. [12]. Rather than the aerodynamics, the scope of this paper focuses on the impact on noise generation and potential structural excitation, which is typically difficult to predict accurately, especially for nonsynchronous flow excitations.

Experimentally, however, the fast response aerodynamic probe technology enables highly accurate flowfield measurements with a bandwidth of 48 kHz. The high temporal resolution of the probe relative to machine characteristics like the blade-passing frequency in combination with fine measurement grids of approximately 1700 points per measurement plane are proven to capture unsteady flow features in great detail. Due to the large amount of data and due to usage of the probe in a virtual four sensor mode, it is required, however, to apply a phase-lock averaging in order to obtain the main flow quantities like total and static pressure, flow angles, and Mach number. Using the rotor rotation as a reference therefore leaves all fluctuations in the data, which are integer multiples of the rotational speed (engine orders). However, for noise and structural considerations, the whole spectrum and (especially) the low-frequency content are of interest. The signal decomposition [29] into a time-mean pressure \bar{p} , a periodic part $\tilde{p}(t)$ and a stochastic part $p'(t)$, according to Eq. (1), is suitable to identify flow regions containing fluctuations not related to the rotational speed. The periodic part of the signal is obtained by dividing the signal into N revolutions at the same rotor/stator position and then ensemble averaging the pieces:

$$p(t) = \bar{p} + \tilde{p}(t) + p'(t) \quad (1)$$

To not lose any frequency content, the raw signal of the yaw sensor $p_1(t)$ is used to calculate the difference to the phase-lock-averaged signal. In this position, the yaw sensor is aligned to the mean flow direction determined by pneumatic probe measurements. The value of $p_1(t)$ is therefore representative of the unsteady total pressure. As indicated by Eq. (2), the root mean square $p'_{1,RMS}$ of the resulting difference $p'_1(t)$ returns increased values if there are fluctuations present in the signal other than engine orders (EOs). The values for $p'_{1,RMS}$ are typically calculated for three rotor blade-passing periods, and the root mean square is calculated from $N = 85$ instants in time when the rotor is at the same relative position to the stator, i.e., once per revolution:

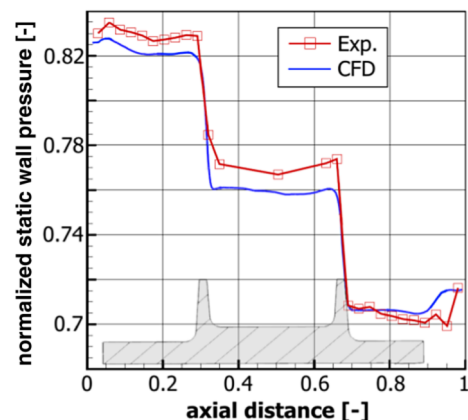


Fig. 6 Comparison between CFD and experiment of normalized static wall pressure at shroud casing.

$$p'_{1,\text{RMS}}(0 \leq t < 3/f_{\text{blade passing}}) = \sqrt{\frac{1}{N} \sum_{i=0}^{N-1} (p(t + i/f_{\text{rot}}) - \bar{p} - \bar{p}(t + i/f_{\text{rot}}))^2} \quad (2)$$

A. Nonsynchronous Flow Perturbations

The most apparent fluctuations in turbomachines are inherent to their working principle: Tonal noise and structural excitation are caused due to the superposition of moving potential fields as well as periodic flow perturbations like wakes or shocks and their interaction with rotating or stationary parts. These features associated to the respective blade-passing frequencies (i.e., the number of blades multiplied by the rotational speed) and the governing aerodynamics can be captured well in experiments as well as unsteady RANS codes with periodic flow domains. Due to the vast amount of research on these topics in the past, the main interactions of stationary and rotating blade rows are well understood. Low-frequency excitation orders and the low harmonics of the rotational speed are typically associated with upstream struts or manufacturing and assembly tolerances like rotor whirl, axial runout, and so on.

In turbines, nonsynchronous fluctuations can be distinguished into tonal and broadband types. Typically, broadband fluctuations are associated with turbulence, like in boundary layers and blade wakes, secondary flows, or jets. The spectrum for this type of fluctuation varies, depending on the source of the turbulence and the relative probe position in both bandwidth and amplitude, but it generally ranges from low engine orders (1, 2, ...) to the blade-passing frequency (BPF) harmonic. More discrete frequencies are found in cavities, wake shedding, and other instabilities, like vortex interaction, swirl instability, acoustic resonances, and others. Elevated values of $p'_{1,\text{RMS}}$ indicate the presence of such nonsynchronous features and point to specific areas in the flow that will be analyzed in more detail in the frequency domain using a Fourier transform. The reference value for $p'_{1,\text{RMS}}$ in the freestream region at the inlet of the turbine is determined to be 35 Pa. Since the fluctuations encountered at the exit of the first stator are of a broadband nature in the wake and secondary flow regions, they are not presented in detail here. The typical subharmonic frequencies encountered at nonzero purge flow injection rates (IRs) in the hub rim seal cavity were described by Schuepbach et al. [22] for a narrower cavity opening. Due to the wider interaction area between the cavity flow and main flow, the dominant fluctuation is the blade-passing frequency rather than the subharmonics for this cavity geometry, which was described in more detail by Jenny et al. [23].

To get the whole spectral information, $p'_{1,\text{RMS}}$ is plotted in the stationary frame of reference at the rotor exit of the baseline case in Fig. 7a. Features associated to the rotor therefore leave a band of elevated fluctuations in the pitchwise direction, whereas stationary features can be pinpointed in this graph. The position of the downstream stator leading edge is indicated by the inclined dashed line. Compared to the reference unsteadiness of 35 Pa at the turbine inlet, the periodic passing of the rotor wake and secondary flows increases the level of unsteadiness at the rotor exit by factors of 30–100. Although their occurrence is periodic, the overall level of unsteadiness is also enhanced compared to the turbine inlet due to the elevated turbulence levels in these flow structures. The circumferential band of elevated unsteadiness from 20 to 40% of the blade span is associated with the passing of the rotor hub passage vortex. The previous research of Jenny et al. [23] showed that the injected purge flow between the hub of stator 1 and the rotor was accumulated inside the passage vortex, and therefore increased the pressure fluctuations in this area. The longer residence time of the vortex in the area of the stator 2 passage and the rather quick swing around the leading-edge potential field result in the peak unsteadiness value of the hub passage vortex in region 1 of Fig. 7a. The radial migration along the pitch is also related to blade–row interaction and the modulation of the purge flow injection at the rotor inlet.

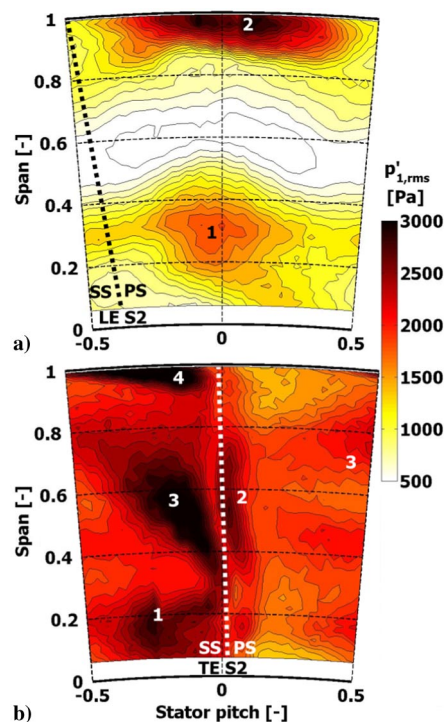


Fig. 7 Time-averaged $p'_{1,\text{rms}}$ at a) rotor exit and b) stator 2 exit for the baseline case.

Previously, Rebholz et al. [12] identified the outflow of overtip leakage fluid from the shroud cavity close to the tip endwall using unsteady total temperature measurements. The region with the peak value of $p'_{1,\text{RMS}}$ coincided with this region in the midpassage of the second stator indicated as 2. Since cavities were known to exhibit instabilities, and since the cavity outflow (like the probe) was bound to the stationary frame of reference, region 2 was of special interest and will be analyzed more in detail later on in the paper.

The mean level of unsteadiness is enhanced even further at the exit of the second stator, as shown in Fig. 7b. The signatures of the wake and secondary flows of stator 2 show clearly, as well as convected structures of the rotor. The hub passage vortex of stator 2 is located in region 1 and the parts of the wake in region 2. The total temperature measurements from the previous study [12] show an accumulation of fluid from the rotor tip secondary flows, as well as rotor overtip leakage fluid in regions 3 and 4. The level of unsteadiness is even higher in these regions than at the associated locations at rotor exit. Therefore, the pressure fluctuations are not decaying through the vane row but accumulate convectively and are potentially amplified. Interestingly, the highest value of $p'_{1,\text{RMS}}$ is found downstream of the second stator. In region 4, where the stator 2 tip passage vortex, the boundary layer, as well as the wake are also interacting with shroud leakage fluid, values of up to 3600 Pa are encountered, which are more than 100 times the level at the inlet of the turbine.

The transformation in the frequency domain reveals sources of the enhanced unsteadiness levels described in the previous section. The pressure signal in the area of the rotor hub passage vortex in Fig. 8a contains only two distinct amplitude peaks between 0 and 5000 Hz, which are normalized by the inlet total pressure: at the rotor blade-passing frequency (2430 Hz) and its second harmonic. The increased unsteadiness level in Fig. 7 originates in a broadband perturbation, which is more than four times higher in this area than in the freestream at midspan. The dynamics of the ingested purge flow as well as the passage vortex behavior lead to a redistribution of energy from the blade-passing frequency and its harmonics to the whole spectrum. Although the freestream reference contains significant fluctuations up to the fifth BPF harmonic, the hub passage vortex area amplitudes at these frequencies are reduced by factors of 2.5 above the second harmonic. This type of signal behavior is expected for the comparison with a highly periodic flow region, like

the wake passing at midspan. Contrary to the blade wakes, the vortical structures close to the hub (and tip) need to be analyzed individually per blade passage to distinguish enhanced turbulence from nonperiodicity. However, in order to resolve the vortex dynamics in more detail, an unfeasibly high sampling frequency will be required (greater than 50 MHz). The frequency analysis of the shroud leakage is shown in Fig. 8b. Compared to the freestream and hub area, several new features can be identified:

1) The amplitude peak at EO1 reaches up to 25% of the BPF amplitude at midspan. Rotor whirl and out of roundness of the casing result in an estimated shroud sealing gap variation of 2–5%, which is suspected to be the main driver of a first-engine-order fluctuation inside the shroud cavity.

2) A nonsynchronous excitation appears around 244 Hz in the region that is associated with shroud leakage. The peak strength of this mode is 30% of the blade-passing amplitude at midspan, and therefore represents a significant noise and excitation source. The maximum amplitude of the nonsynchronous excitation is found in the same location as the maximum unsteadiness values $p'_{i,RMS}$. The depicted point is chosen offcenter of the extremum because the features described in the next paragraph are not as pronounced as in the border region of the shroud leakage.

3) Both the EO1 mode and the nonsynchronous mode appear to interact in a nonlinear way with the rotor blade-passing frequency, since mirror images of the different frequencies can be found at the blade passing plus and minus 45 and 244 Hz. Since the low-frequency excitation of the flow appears only in flow regions that are strongly influenced by the shroud exit cavity, a detailed analysis of the cavity excitation will be presented in a later section.

Similar to the broadband fluctuations found in the hub passage vortex region at the rotor exit, regions 1 (stator 2 hub passage vortex) and 2 (stator 2 wake) in Fig. 7b show elevated pressure amplitudes over the whole spectrum with similar magnitudes as at the rotor exit (five times the freestream turbulence at rotor exit). Parts of the rotor blade-passing fluctuations are reduced by the convection through the second stator, since significant amplitudes of the rotor blade-passing frequency only appear up to the second harmonic (fifth harmonic at rotor exit). Since the tip secondary flows and shroud leakage are

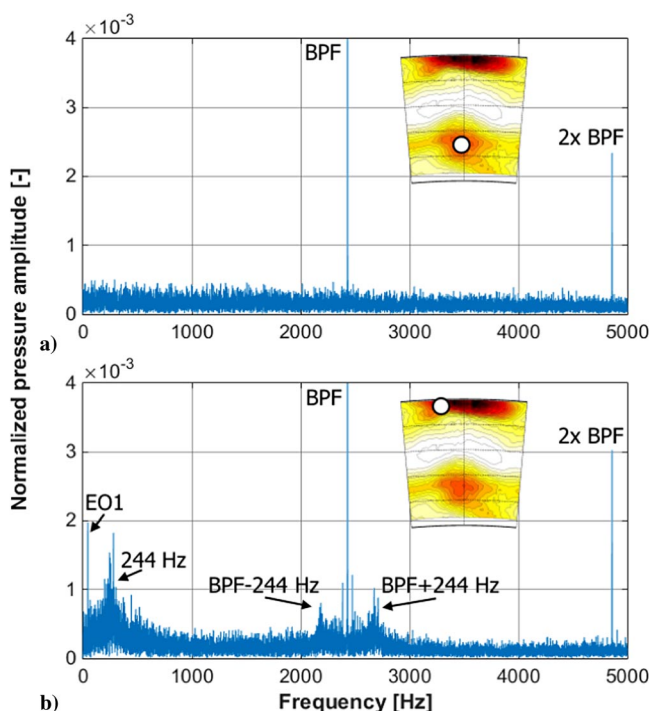


Fig. 8 Normalized Fourier transform of pressure at rotor exit for the baseline configuration.

accumulated around the midspan on the suction side of the second stator, the presence of the low-frequency fluctuation around 244 Hz in Fig. 9a can be related to the upstream leakage fluid. The amplitudes of both the first engine order as well as the nonsynchronous mode are not reduced significantly through the vane row, and therefore represent a noise source or excitation source for downstream rows. Figure 9b shows the amplitude spectrum in the interaction region of the stator 2 tip passage vortex and the tip endwall boundary layer at the stator 2 exit. The peak amplitude in this area can be found at 233.5 Hz and is approximately 1.5 times higher than the rotor blade-passing amplitude at midspan at the rotor exit. This mode therefore represents one of the highest fluctuations found in the turbine flowfield. Zooming in on the frequency band from 0 to 500 Hz also shows multiple distinct peaks in the vicinity of the resonance at 233.5 Hz at 20–25 Hz intervals. Contrary to this mode, the cavity resonance at the rotor exit has a comparably smooth amplitude distribution around the resonance. Since the leakage oscillation frequency covers the frequency band of this instability, it is apparent that the nonsynchronous fluctuation of the shroud leakage flow excites a flow instability in the area of the stator 2 tip secondary flow formation. A qualitative time-frequency analysis using the short time Fourier transform shows that the peak shape of the shroud leakage oscillation at the rotor exit varies significantly over time, and therefore results in the rather broad amplitude distribution around 244 Hz. The frequency associated to the peak at 233.5 Hz in Fig. 9b is found to be more constant over time. This behavior supports the conclusion that the shroud leakage oscillations excite a separate instability in the tip secondary flows of the second stator. Further, the fast Fourier transformation applied to the signal is expected to underestimate the amplitudes in the nonstationary fluctuations in the shroud leakage area.

B. Low-Frequency Noise Reduction Using a Partial Shroud

To verify the origin of the nonsynchronous low-frequency oscillations to be within the shroud cavity, the unsteady wall pressure at the shroud casing is analyzed for different shroud geometries. Figure 10 shows the amplitude spectrum at the 91.3% axial cavity length for the baseline, the LE cutback, and the TE cutback. The spectra are averaged circumferentially over 40 points. The described

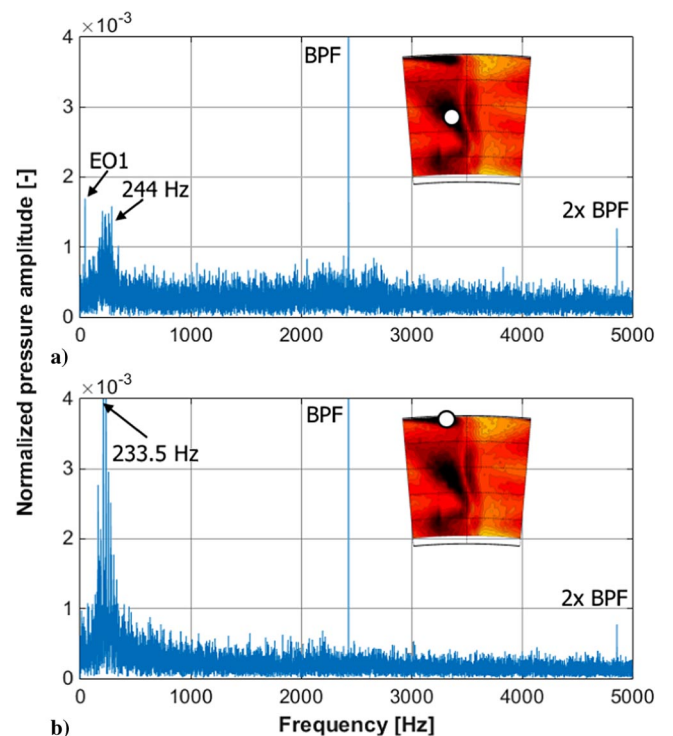


Fig. 9 Normalized Fourier transform of pressure at stator 2 exit for the baseline configuration.

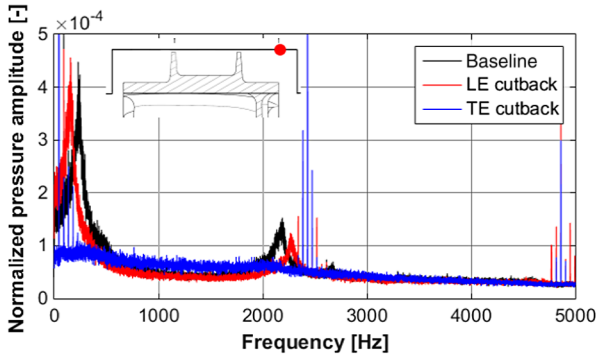


Fig. 10 Fourier transform of the shroud cavity wall pressure.

244 Hz oscillation as well as the difference frequency to the blade-passing frequency measured with the FRAP downstream of the rotor and the second stator can be clearly observed inside the cavity for baseline as well. Due to the circumferential averaging, the signal looks cleaner and the peaks are better distinguishable, but the peak amplitude of the resonance is damped. Compared to the fluctuations in the main flow, the maximum fluctuations at the outer casing wall are approximately half as high. The signature of the low engine orders is enhanced significantly compared to the main flow as well, since their mirror images around the blade-passing frequency are also visible.

The cavity geometry as well as the static pressure at the rotor exit has not changed from the baseline to the LE cutback test case. Therefore, the observed change in resonance frequency for the baseline (244 Hz) and the LE cutback (155 Hz) has to be associated with the changed static pressure drop across the seals. It has been reported in [12] that the pressure drop across the first shroud fin increases by 37% and decreases for the second fin by 13.5% for the LE cutback. Additionally, the shroud inlet cavity flowfield is dominated by the rotor flowfield. The excitation of the exit cavity flow structures is therefore changed for the LE cutback and leads to a shift of 90 Hz for the oscillation frequency and the difference frequency close to the rotor blade passing.

Similar to the inlet cavity for the LE cutback, the flowfield in the exit cavity of the TE cutback is dominated by the rotor blade passing. The rotor-bound fluid exchange with the main flow was also described in [12]. Due to the dominance of the rotor blade-passing frequency, no nonsynchronous excitations are present in the shroud exit cavity for the TE cutback. However, the enhanced fluid exchange with the main flow compared to the baseline leads to an increased broadband amplitude level up to the blade-passing frequency.

According to numerical estimations in [12], the tip shroud seals are not choked. In the subsonic flow across the seals, acoustic modes will be able to communicate between the three cavities. Acoustic resonances of the cavities will therefore be equally visible along the whole shroud, and possibly even upstream in the main flow at rotor inlet. Typical mode shapes will be axial standing waves as well as pitchwise rotating modes. Due to the complex boundary conditions at the interfaces to the main flow, and due to the presence of low-frequency modulation by the lowest engine orders (especially close to gaps), the accurate prediction of the frequency of such modes is unfeasible with most commercial tools. Figures 11a and 11b indicate the presence of the low-frequency oscillations at 244 Hz for the baseline and 155 Hz for the LE cutback case only in the exit cavity downstream of the second seal. Given the nonchoked flow across the seals, an acoustic resonance can be excluded as a source for the oscillation. The rotor whirl and eccentricity of the rotor casing dominate the pressure oscillation in the vicinity of the shroud seals and can presumably be related to the onset of the low-frequency oscillations in the shroud exit cavity. Despite the presence of high first-engine-order fluctuations across the second seal for the TE cutback in of Fig. 11c, no low-frequency content is detected in the exit cavity. The amplitude of the rotor blade-passing frequency is

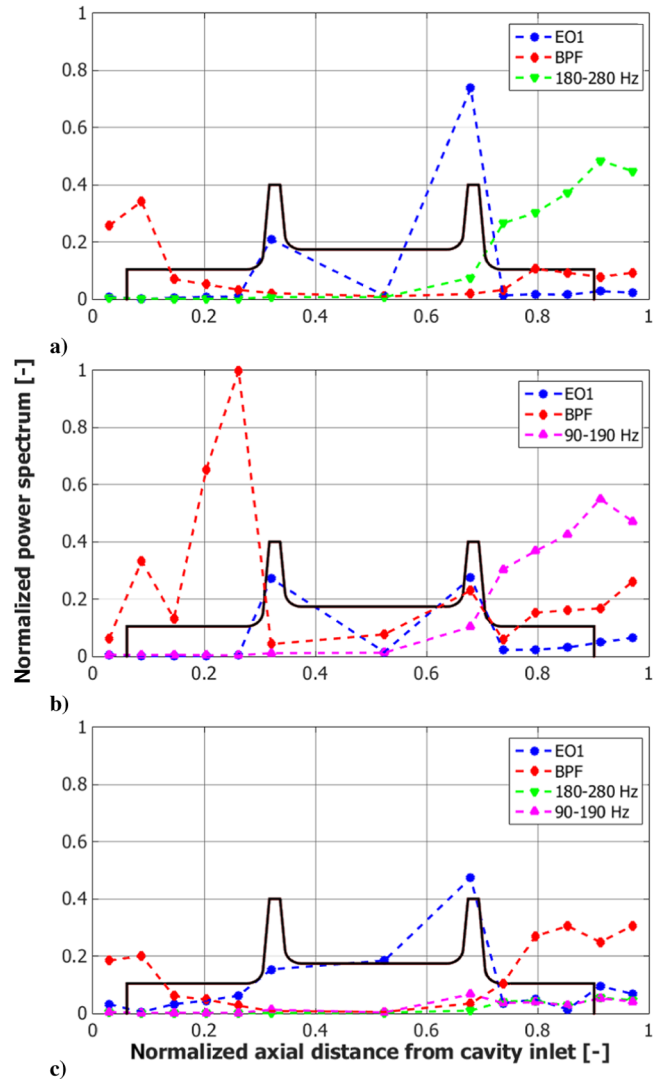


Fig. 11 Normalized power spectrum of casing pressure for a) baseline, b) LE cutback, and c) TE cutback.

more than twice as high than for the other test cases and extends upstream from the cavity exit almost up to the second seal, and therefore enforces a more periodic rotor-bound flowfield inside the cavity. The remaining frequency content in the two bands from 90 to 190 Hz and 180 to 280 Hz is marginal and can be attributed to enhanced broadband fluctuations.

In addition to the altered pressure drop across the two shroud sealing fins, the potential cavity excitation mechanism in the LE cutback case is different when compared to the baseline. The rotor blade-passing frequency is dominant at the first fin due to the rotor-locked fluid injection; therefore, it is also enhanced in the intermediate cavity as well as across the second fin. Contrary to the TE cutback, the oscillations at the rotor blade-passing frequency do not originate at the cavity exit but are transmitted through the seals. Given the findings in [12], this can be attributed to the periodic variation of stagnation pressure at the seals caused by the radial inflow jets in the inlet cavity.

Figure 12 shows the evolution of the difference frequency as a function of rotor pressure drop. Due to the entanglement with the first to third engine order, the low-frequency oscillations are difficult to extract separately at various measurement points. Therefore, the nonlinear coupling frequency, which is the difference between the low-frequency oscillations and the blade-passing frequency, is depicted here for the LE cutback. A pressure drop of one indicates the nominal operating point. Since the data are not averaged circumferentially and recorded at a different axial location than the data in

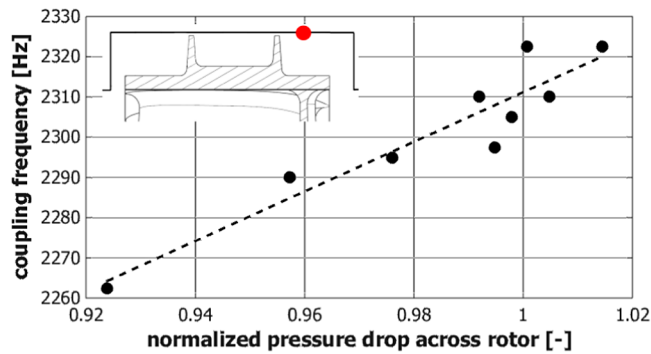


Fig. 12 Nonlinear coupling frequency maximum for different rotor pressure drops for the LE cutback case.

Fig. 10, the frequency deviates by approximately 20 Hz. Figure 12 shows a linear coupling of the difference frequency (and therefore the low-frequency oscillation) and the pressure drop across the rotor. Compared to the change in pressure drop across the rotor, the exit static pressures at the rotor tip and, therefore, the shroud exit cavity static pressure are relatively constant for the different test cases. At the same inlet total temperature to the turbine, the density in the exit cavity also remains approximately constant, i.e., an acoustic resonance cannot explain the frequency shifts. Overall, swirl and vortical instabilities are therefore the most likely sources for the low-frequency mode, since they are closely related to leakage mass flow and seal jet velocity.

The consequences of all shroud cutbacks at the turbine exit for the two most prominent oscillations (the cavity frequency and the blade-passing frequency) are summarized in Fig. 13. The peak pressure fluctuation intensity change relative to the baseline is shown at the stator 2 exit for the cavity frequency range of 100–350 Hz in Fig. 13a. Close to the hub, none of the shroud modifications shows a significant impact, since this area is dominated by the stator 2 and rotor hub flowfield, which is not affected notably by the shroud modifications. The absence of the cavity mode starts showing for the shroud trailing-edge modifications in the accumulation zone of rotor tip secondary flows and overtip leakage on the suction side of the second stator above a 30% span. Although the LE cutback remains close to the baseline intensity level, the TE and the combined cutback show a reduction of approximately 7 dB at midspan. Due to the excitation of an instability in the area of the stator 2 tip passage vortex and boundary-layer interaction at 233 Hz, the intensity peaks

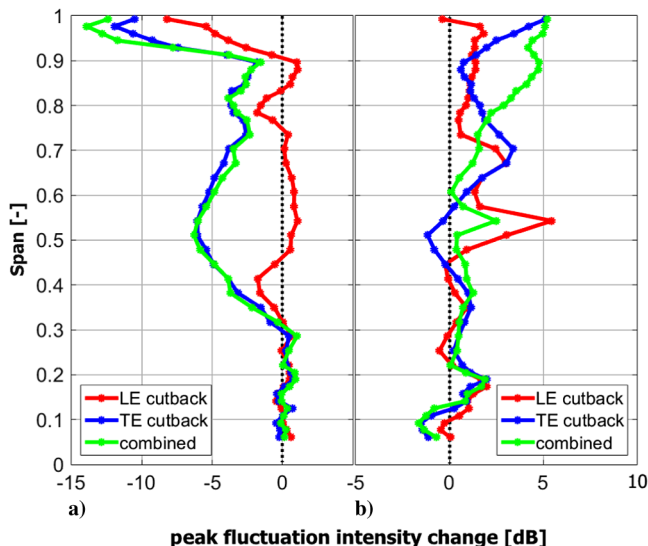


Fig. 13 Spanwise peak intensity change at stator 2 exit for a) 100–350 Hz and b) BPF.

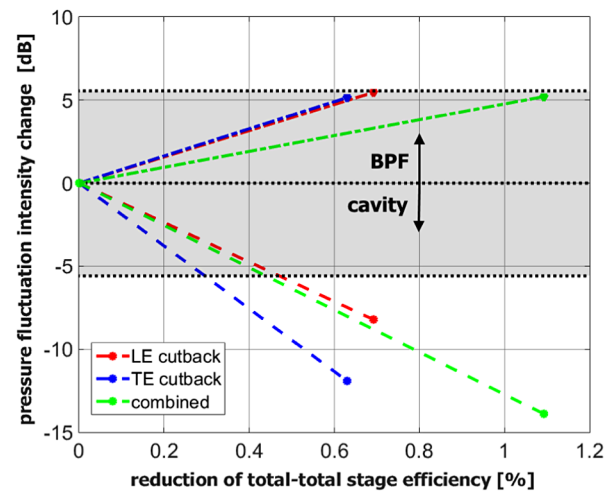


Fig. 14 Stator 2 exit pressure intensity change of the BPF and the cavity mode (100–350 Hz).

for the baseline close to the endwall. Since LE cutback cavity frequency is around 155 Hz, this instability in the second vane row is not triggered; therefore, a reduction in the peak fluctuation intensity of 8 dB at the tip endwall is found. The TE cutback and the combined cutback feature identical modifications to the shroud trailing-edge platform, and they show a reduction in fluctuation intensity of 12 dB for the TE cutback and 14 dB for the combined cutback when compared.

Figure 13b shows the spanwise evolution of the other dominant tonal fluctuation component: the blade-passing frequency. On average, all cutbacks create higher fluctuations due to the alteration of the rotor secondary and leakage flows. The fluctuation intensity increases on average by less than 3 dB and peaks close to the tip endwall at 5 dB for the two cases featuring a trailing-edge modification. Considering the maximum fluctuation amplitude at the stator 2 exit as a potential noise source in the last stages of a low-pressure turbine, Fig. 14 illustrates the tradeoff between a total-total stage efficiency drop and a reduction in tonal noise generation. The maximum increase in intensity is rather constant for all cutbacks at around 5–6 dB. However, the shaded area indicates that the cavity fluctuation reduction outweighs the increase at the blade-passing frequency. If the design priority is put on noise emission, like in the last stages of a low-pressure turbine, a shroud trailing-edge cutback therefore represents an effective tool to reduce low-frequency noise generation. As presented in [12], this particular TE cutback design reduces the total-to-total stage efficiency by 0.7%, resulting in the best tradeoff of all cutbacks.

C. Numerical Prediction of Nonsynchronous Cavity Modes

With increasing computational power, computational fluid dynamics has become an integral part of the engine design process. To resolve all relevant flow features for a reasonably accurate prediction of turbine efficiency using unsteady Reynolds-averaged Navier–Stokes equations, the flow domain still has to be divided into periodic sectors with conventional methods. The periodicity in the circumferential direction acts physically as a high-pass filter for pitchwise fluctuations, i.e., only pressure waves with wavelengths of $\lambda = 2/n$ pitch, $n = 1, 2, \dots$, for standing waves and $\lambda = 1/n$ pitch for travelling waves can be sustained. Making use of the computational acceleration of up to 30 times [18] on GPUs allows simulation of a full 360 deg model without any periodic assumption.

The buildup of low-frequency modes requires more simulation time than the inherent oscillation, like blade-passing events. Figure 15 shows the Fourier transform of the pressure signal in the shroud exit cavity for the baseline case after 2.7 full rotor revolutions for the latest 300 time steps. Next to the rotor blade-passing frequency, an amplitude peak between 1500 and 2000 Hz can be observed. The frequency does not match the dominant mode

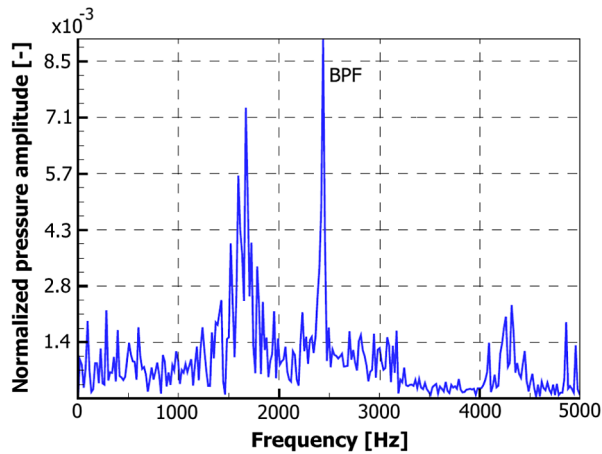


Fig. 15 Fourier transform of the normalized shroud exit cavity pressure in the full-annular simulation of the baseline.

observed in the experiment. Also, the nonlinear coupling with the blade-passing frequency does not show. The analysis of the three-dimensional flowfield does not point out a clear source of this oscillation. In comparison with the experiment, the absence of the first engine orders is also apparent, since assembly tolerances are not modeled.

Typical convergence criteria like the periodic correlation for two blade-passing events do not apply necessarily to cavities in full-annular simulations. Although the main flow is well converged, judging from the periodic correlation, Fig. 16 clearly indicates that the amplitude variation in the cavity has not stabilized, even after 3.25 simulated rotor revolutions. Interestingly, this is also true for the blade-passing frequency. Since the amplitudes in the frequency band from 1500 to 2000 Hz do not show a decaying trend, and since no peaks start to build up around 244 Hz, the simulation is stopped at this point. From the initial guess, which is taken from periodic simulations, the amplitudes of both the rotor passing frequency as well as the frequency band around 1.75 kHz decrease rather steadily for about one full rotor revolution. Afterward, the amplitudes exhibit a more fluctuating character. The variation in amplitude does not, as pointed out previously, necessarily mean that flow is not converged yet. However, the general trend of the pressure amplitudes is rising over several revolutions, and since the experimental data do not indicate any significant oscillations below the first engine order, a convergence issue cannot be excluded in this case. The shorter periods of these fluctuations are not constant in the observed time but in the order of a rotor revolution. This suggests that the presence of the first and second engine orders with comparable amplitudes will alter the behavior in the shroud cavity significantly.

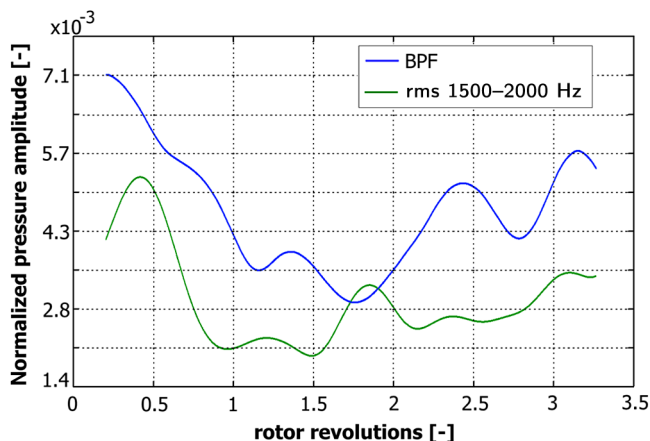


Fig. 16 Time history of the two dominant pressure amplitudes in the simulated full-annular shroud exit cavity for the baseline.

V. Conclusions

From the extensive probing of four different tip shroud configurations, the fully shrouded rotor emerged as the aerodynamically most efficient one. Since the optimization of noise emissions and the part lifetime has become an integral part of the design procedure of modern aeroengines, an extended analysis of the turbine flowfield has been carried out in the frequency domain. In addition to the rotor-stator interaction, which was well captured in standard processing methods, a nonsynchronous instability in the shroud exit cavity at 244 Hz was identified. The propagation into the main flow resulted in amplitudes of 30% of the rotor blade-passing frequency at the rotor exit. The perturbations were convected almost without attenuation through the downstream vane row and excited an instability at 233 Hz in the interaction area between stator tip secondary flows and the boundary layer. The order of magnitude of the resulting fluctuations at the turbine exit exceeded the blade-passing frequency amplitude at the rotor exit by up to 50%. The dependency on the pressure drop across the second rotor shroud seal resulted in a variation of the cavity frequency, and therefore excluded acoustic resonances as an excitation source rather than swirl or vortex instabilities. This was also supported by the observation that the modes occurred only in the exit cavity and did not propagate in the adjacent cavities, although the seals were not choked. Due to the reduced cavity frequency (155 Hz) with the LE cutback case, the instability in the second stator was not triggered.

Although the constraint of periodic boundaries is omitted for a full-annular unsteady CFD simulation, the low-frequency dynamics cannot be resolved numerically. The dominance of the first-engine-order excitation in the seal gaps cannot be modeled with conventional CFD methods. However, due to the proximity to the cavity modes, low engine orders might well be responsible for the excitation of the nonsynchronous mode.

The dominance of the rotor flowfield suppresses the creation of any cavity dynamics completely for shroud trailing-edge cutbacks. The absence of the cavity modes results in a reduction of low-frequency peak amplitudes at the turbine exit by 12 dB for the TE cutback at a total-total stage efficiency reduction of 0.7% compared to the baseline. Since the prediction of the cavity modes is found to be difficult, the application of shroud trailing-edge cutbacks appears as a viable measure to suppress low-frequency oscillations, which are typically associated with combustion chambers, and therefore not budgeted in the acoustic design of a low-pressure turbine. The high amplitude of these fluctuations and the low attenuation through blade rows represent a considerable excitation source for both structural vibrations as well as the emission of additional tonal noise from the exhaust of a jet engine.

Acknowledgments

The work leading to the results of this paper was carried out within the joint industrial and academic research program that is part of the "Luftfahrtforschungsprogramm LuFo IV" (reference number 20T0810) supported by the German Federal Ministry of Economics and Technology. The first author would also like to thank P. Plagowski for his support during the data analysis.

References

- [1] Wu, X., Vahdati, M., Schipani, C., and Imregun, M., "Analysis of Low-Pressure Turbine Flutter for Different Shroud Interfaces," *Proceedings of the ASME Turbo Expo*, American Soc. of Mechanical Engineers Paper GT2007-27377, Fairfield, NJ, 2007.
- [2] Kurzke, J., "Fundamental Differences Between Conventional and Geared Turbofans," *Proceedings of the ASME Turbo Expo*, American Soc. of Mechanical Engineers Paper GT2009-59745, Fairfield, NJ, 2009.
- [3] Lyon, T. A., and Hillery, R. D., "Geared Fan Engine Systems—Their Advantages and Potential Reliability," *Journal of Aircraft*, Vol. 10, No. 6, June 1973, pp. 361–365. doi:10.2514/3.60237
- [4] Harvey, N. W., "Aerothermal Implications of Shrouded and Shrouded Blades," *VKI Lecture Series on Turbine Blade Tip Design and Tip*

- Clearance Treatment*, von Kármán Inst. for Fluid Dynamics Sint-Genesius-Rode, Belgium, 2004, pp. 1–120.
- [5] Kaiser, I., and Bindon, J. P., “The Effect of Tip Clearance on the Development of Loss Behind a Rotor and a Subsequent Nozzle,” American Soc. of Mechanical Engineers Paper 1997-GT-053, Fairfield, NJ, 1997.
- [6] Camci, C., Dey, D., and Kavurmacioglu, L., “Aerodynamics of Tip Leakage Flows near Partial Squealer Rims in an Axial Flow Turbine Stage,” *Journal of Turbomachinery*, Vol. 127, No. 1, 2005, pp. 14–24. doi:10.1115/1.1791279
- [7] Mischo, B., Behr, T., and Abhari, R. S., “Flow Physics and Profiling of Recessed Blade Tips: Impact on Performance and Heat Load,” *Journal of Turbomachinery*, Vol. 130, No. 2, 2008, Paper 021008.
- [8] Dey, D., and Camci, C., “Aerodynamic Tip De-Sensitization of an Axial Turbine Rotor Using Tip Platform Extensions,” American Soc. of Mechanical Engineers Paper 2001-GT-484, Fairfield, NJ, 2001.
- [9] Zhou, C., Hodson, H., Tibbott, I., and Stokes, M., “Effects of Winglet Geometry on the Aerodynamic Performance of Tip Leakage Flow in a Turbine Cascade,” *Journal of Turbomachinery*, Vol. 135, No. 5, 2013, Paper 051009.
- [10] Nirmalan, N. V., and Bailey, J. C., “Experimental Investigation of Aerodynamic Losses of Different Shapes of a Shrouded Blade Tip Section,” *Proceedings of the ASME Turbo Expo*, American Soc. of Mechanical Engineers Paper GT2005-68903, Fairfield, NJ, 2005.
- [11] Porreca, L., Kalfas, A. I., and Abhari, R. S., “Aerothermal Analysis of a Partially Shrouded Axial Turbine,” *Journal of Power and Propulsion*, Vol. 25, No. 1, 2009, pp. 181–190. doi:10.2514/1.34902
- [12] Reholz, P. S., Kalfas, A. I., Abhari, R. S., and Zscherp, C., “Experimental and Numerical Study of the Impact of a Tip Shroud Leading and Trailing Edge Cutback on the Efficiency of a Low Pressure Gas Turbine Stage,” *International Society on Airbreathing Engines (ISABE)*, ISABE Paper 2013-1159, 2013.
- [13] Bushell, K. W., “A Survey of Low Velocity and Coaxial Jet Noise with Application to Predictions,” *Journal of Sound and Vibration*, Vol. 17, No. 2, 1971, pp. 271–282. doi:10.1016/0022-460X(71)90461-5
- [14] Gezork, T., Mayorca, M. M., Groth, P., Vogt, D. M., and Fransson, T., “Influence of Tip Shroud Cavity Detailing on Turbine Blade Forcing Calculations,” American Soc. of Mechanical Engineers/IGTI Paper GT2014-26724, 2014.
- [15] Barmpalias, K. G., Kalfas, A. I., Abhari, R. S., Hirano, T., and Shibukawa, N., “Effects of Design Variations of Rotor Entry Cavity Geometry on Shrouded Steam Turbine Performance,” *Proceedings of the ASME Turbo Expo*, American Soc. of Mechanical Engineers/IGTI Paper GT2010-22279, Fairfield, NJ, 2010.
- [16] Blackburn, H. M., and Lopez, J. M., “Modulated Waves in a Periodically Driven Annular Cavity,” *Journal of Fluid Mechanics*, Vol. 667, Jan. 2011, pp. 336–357. doi:10.1017/S0022112010004520
- [17] Globulev, V. V., and Atassi, H. M., “Acoustic-Vorticity Waves in Swirling Flows,” *Journal of Sound and Vibration*, Vol. 209, No. 2, 1998, pp. 203–222.
- [18] Basol, A. M., Raheem, A., Huber, M., and Abhari, R. S., “Full-Annular Numerical Investigation of the Rim Seal Cavity Flows Using GPU’s,” American Soc. of Mechanical Engineers/IGTI Paper GT2014-26755, 2014.
- [19] Karabasov, S. A., Hynes, T. P., and Dowling, A. P., “Effect of Mean-Flow Evolution on Sound Propagation Through Non-Uniform Jet Flows,” AIAA Paper 2007-3655, 2007.
- [20] Nebenfuhr, B., Yao, H., Peng, S.-H., and Davidson, L., “Hybrid RANS/LES Simulations for Aerodynamic and Aeroacoustic Analysis of a Multi-Element Airfoil,” AIAA Paper 2013-2066, 2013.
- [21] Behr, T., Kalfas, A. I., and Abhari, R. S., “Unsteady Flow Physics and Performance of a One-and-1/2-Stage Unshrouded High Work Turbine,” *Journal of Turbomachinery*, Vol. 129, No. 2, June 2008, pp. 348–359.
- [22] Schuepbach, P., Abhari, R. S., Rose, M. G., and Gier, J., “Sensitivity of Turbine Efficiency and Flow Structures to Varying Purge Flow,” *Journal of Propulsion and Power*, Vol. 26, No. 1, 2010, pp. 46–56. doi:10.2514/1.44646
- [23] Jenny, P., Abhari, R. S., Rose, M. G., Brettschneider, M., and Gier, J., “A Low Pressure Turbine with Profiled End Walls and Purge Flow Operating with a Pressure Side Bubble,” *Journal of Turbomachinery*, Vol. 134, No. 6, 2012, pp. 1–9. doi:10.1115/1.4006303
- [24] Porreca, L., Kalfas, A. I., and Abhari, R. S., “Optimized Shroud Design for Axial Turbine Aerodynamic Performance,” *Journal of Turbomachinery*, Vol. 130, No. 3, July 2008, Paper 031016. doi:10.1115/1.2777187
- [25] Kupferschmied, P., Kopperl, O., Gizzi, W. P., and Gyarmathy, G., “Time Resolved Flow Measurements with Fast Aerodynamic Probes in Turbomachinery,” *Journal of Measurement Science and Technology*, Vol. 11, No. 7, 2000, pp. 1036–1054. doi:10.1088/0957-0233/11/7/318
- [26] Pfau, A., Schlienger, J., Kalfas, A. I., and Abhari, R. S., “Unsteady 3-Dimensional Flow Measurement Using a Miniature Virtual 4-Sensor Fast Response Aerodynamic Probe (FRAP),” *Proceedings of the ASME Turbo Expo*, American Soc. of Mechanical Engineers/IGTI Paper GT2003-38128, Fairfield, NJ, 2003.
- [27] Behr, T., “Control of Rotor Tip Leakage and Secondary Flow by Casing Air Injection in Unshrouded Axial Turbines,” Ph.D. Dissertation, Swiss Federal Institute of Technology, Zurich, Switzerland, 2007, No. 17283.
- [28] Ni, R., “A Multiple-Grid Scheme for Solving the Euler Equations,” *AIAA Journal*, Vol. 20, No. 11, 1981, Paper 1025R.
- [29] Porreca, L., Hollenstein, M., Kalfas, A. I., and Abhari, R. S., “Turbulence Measurements and Analysis in a Multistage Axial Turbine,” *Journal of Propulsion and Power*, Vol. 23, No. 1, Jan.–Feb. 2007, pp. 227–234.

T. J. Praisner
Associate Editor